Received: 18 June 2020 | Revised: 9 October 2020 | Accepted: 13 October 2020

DOI: 10.1002/mrm.28582

FULL PAPER

Magnetic Resonance in Medicine

An optimized b-value distribution for triexponential intravoxel incoherent motion (IVIM) in the liver

Andreas Riexinger[1] | **Jan Martin**[1] | **Andreas Wetscherek**[2] | **Tristan Anselm Kuder**[3] | **Michael Uder**[1] | **Bernhard Hensel**[4] | **Frederik Bernd Laun**[1]

[1]Institute of Radiology, University Hospital Erlangen, Erlangen, Germany

[2]Joint Department of Physics, The Institute of Cancer Research and The Royal Marsden NHS Foundation Trust, London, United Kingdom

[3]Department of Medical Physics in Radiology, German Cancer Research Center (DKFZ), Heidelberg, Germany

[4]Center for Medical Physics and Engineering, Friedrich-Alexander-Universität Erlangen-Nürnberg (FAU), Erlangen, Germany

Correspondence
Andreas Riexinger, Institute of Radiology, University Hospital Erlangen, Maximiliansplatz 3, D-91053 Erlangen, Germany.
Email: andreas.riexinger@uk-erlangen.de

Funding information
Deutsche Forschungsgemeinschaft (DFG), Grant/Award Numbers: LA 2804/12-1 and LA 2804/13-1

Purpose: To find an optimized b-value distribution for reproducible triexponential intravoxel incoherent motion (IVIM) exams in the liver.

Methods: A numeric optimization of b-value distributions was performed using the triexponential IVIM equation and 27 different IVIM parameter sets. Starting with an initially optimized distribution of 6 b-values, the number of b-values was increased stepwise. Each new b-value was chosen from a set of 64 predefined b-values based on the computed summed relative mean error of the fitted triexponential IVIM parameters. This process was repeated for up to 100 b-values. In simulations and in vivo measurements, optimized b-value distributions were compared to 4 representative distributions found in literature.

Results: The first 16 optimized b-values were 0, 0.3, 0.3, 70, 200, 800, 70, 1, 3.5, 5, 70, 1.2, 6, 45, 1.5, and 60 in units of s/mm^2. Low b-values were much more frequent than high b-values. The optimized b-value distribution resulted in a higher fit stability compared to distributions used in literature in both, simulation and in vivo measurements. Using more than 6 b-values, ideally 16 or more, increased the fit stability considerably.

Conclusion: Using optimized b-values, the fit uncertainty in triexponential IVIM can be largely reduced. Ideally, 16 or more b-values should be acquired.

KEYWORDS

diffusion, intravoxel incoherent motion, liver, MRI, optimization, triexponential

1 | INTRODUCTION

In 1988, Le Bihan et al[1] introduced the intravoxel incoherent motion (IVIM) model to separate perfusion from diffusion effects within an MRI measurement. The measured signal can be described by a biexponential function:

$$\frac{S(b)}{S_0} = (1-f)\cdot\exp(-b\cdot D)+f\cdot\exp\left(-b\cdot D^*\right). \quad (1)$$

The perfusion fraction f quantifies the relative signal of incoherently flowing blood, the pseudo-diffusion coefficient D^* represents blood perfusion, and D is the tissue diffusivity.

$S(b)$ corresponds to the diffusion-weighted and S_0 to the unweighted signal (b = 0 s/mm^2). Because reproducibility in IVIM experiments is a challenge,[2] different methods were suggested to reduce the measurement uncertainty.[3-5] Several optimization schemes have been introduced to improve reproducibility and accelerate data acquisition.[6-9]

Recently, it has been shown that using small b-values (below 10 s/mm^2), the signal decay in some abdominal organs is better described by a triexponential function instead of the more traditional biexponential function:

$$\frac{S(b)}{S_0} = (1-f_1-f_2)\cdot\exp(-b\cdot D) + f_1\cdot\exp\left(-b\cdot D_1^*\right) + f_2\cdot\exp\left(-b\cdot D_2^*\right). \quad (2)$$

Here, f_1 and f_2 represent perfusion fractions, and D_1^* and D_2^* represent the pseudo-diffusion coefficients.[5,10-15] These additionally obtainable quantitative parameters might be useful, for example, to separate benign and malignant lesions as it was demonstrated for biexponential IVIM (e.g., Cho et al and Murtz et al).[16,17] More interesting, however, might be the exploration of the nature of the triexponential IVIM effect, because it could unveil general properties of the IVIM effect. Data published to date suggest that the observed triexponential IVIM curve is rather data representation than a biophysical model in the spirit of Novikov et al's definition.[18] In particular, it seems unlikely that D_1^* and represent true pseudo diffusion processes (in the many-directional changes limit, model 1 by le Bihan et al)[19] because the IVIM effect mostly vanishes if flow-compensated gradients are used (e.g., Wetscherel et al).[20] It also seems unlikely that D_1^* and D_2^* can be linked tightly to arterial and venous compartments because the then expected, B_0 dependency was not observed.[15] A possible explanation is that the IVIM signal decay curve of the perfusion compartments represents $\langle\exp(i\alpha v)\rangle = \int P(v)\exp(i\alpha v)\,dv$, where $\alpha = \gamma\int G(t)\,tdt$ is the flow-weighting generated by the applied gradients $G(t)$, that is, essentially the first gradient moment of the diffusion encoding gradients, and v the velocity. At least in the short-time limit, this should hold true, when blood flow directions do not change during the encoding period. The expectation brackets describe the presence of a velocity distribution $P(v)$ whose shape and origin needs to be further explored. It most presumably has venous, arterial, and capillary contributions. Future studies are needed to explore the nature of $P(v)$ and of the respective blood flow correlation times.

To perform such studies, however, a stable fitting of triexponential IVIM curves is necessary. Estimated fit parameters vary widely across different studies that fitted the triexponential IVIM function (see Table 1). An important aspect to consider is the use of different b-values. Varying the distribution of b-values in the protocol affects the estimates of IVIM parameters.[21,22] In a recent study, b-values down to $b \approx 0.1$ s/mm^2 were used, which led to increased determined pseudo-diffusion coefficients, which is in good agreement with the finding of threshold dependent IVIM parameter in the biexponential case.[23]

Considering the problem of hardly reproducible pseudo-diffusion coefficients[22] and echo time dependent perfusion fractions,[24] the aim of this work was to find optimized b-values that reduce the fit uncertainty in all triexponential IVIM parameters, which are robust at different TEs and for the wide range of pseudo-diffusion coefficients found in liver exams.

TABLE 1 Published triexponential IVIM parameters with a field strength of B_0 = 3T

Publication	Organ	D	D_1^*	D_2^*	f_1	f_2	b-values	TE/TR
Cerceueil et al[10]	Liver	1.35	26.5	404	0.14	0.14	0, 5, 10, 15, 20, 25, 30, 35, 40, 45, 50, 100, 200, 400, 600, 800	67/1rc
Riexinger et al[15]	Liver	1.22	81.3	2453	0.161	0.152	3 × 0.2, 0.4, 0.7, 0.8, 1.1, 1.7, 3, 3.8, 4.1, 4.3, 4.4, 4.5, 4.9, 10, 15, 20, 2 × 30, 50, 60, 90, 90, 95, 2 × 150, 5 × 180, 4 × 500	100/2500
van der Bel et al[11]	Whole kidney	1.9	9.7	551	0.16	0.06	0, 2, 4, 8, 12, 18, 24, 32, 40, 50, 75, 110, 200, 300, 450, 600	61/2068
van Baalen et al[12]	Whole kidney	1.50	5.77	352			0, 10, 25, 40, 75, 100, 200, 300, 500, 700	45/1344
Kuai et al[5]	Liver	1.21	19.32	387	0.17	0.17	0, 5, 15, 25, 35, 50, 100, 200, 400, 600, 800	68/1rc
	Kidney	1.74	13.07	–	0.27	–		
	Spleen	0.75	12.31	179	0.09	0.08		
Wurnig et al[13]	Liver	1.26	43.8	270	0.08	0.13	68 b-values, equally spaced from 0-1005	57/5300
	Kidney cortex	2.26	23.8	264	0.06	0.05		
	Kidney med	1.57	5.23	168	0.36	0.06		
	Spleen	0.91	–	69.8	0.05	–		

D, D_1^*, and D_2^* are stated in 10^{-3} mm^2/s, the b-values in s/mm^2 and TE and TR in ms. 1rc = 1 respiratory cycle.

2 | METHODS

2.1 | Optimization routine

The optimization and all simulations were performed in MATLAB (The MathWorks Release R2017b, Natick, MA). The optimization was performed using the triexponential IVIM Equation 1 as signal equation. To perform the optimization, one must know the typical range of values of the triexponential IVIM parameters. Table 1 provides an overview of currently published values. One thing to note is that D_2^* reported in Riexinger et al[15] is roughly by 1 order of magnitude larger than the D_2^* values reported in the other publications,[5,10,11,13,14] which most likely can be attributed to the lower minimal b-value used in Riexinger et al.[15] The optimization performed here is based on the assumption that these large D_2^* values are a good representation of the real values and that consequently very small b-values, say below 1 s/mm^2, are needed to sample such large D_2^* values. Triexponential IVIM parameters obtained with such very small b-values have so far been reported only for the liver to our knowledge. Consequently the optimization performed here is based on these liver values.

2.2 | Ground truth values

To avoid over-fitting to 1 particular set of triexponential IVIM parameters and to account for the likely spread of values in a patient population, the optimization was based on 27 different combinations of triexponential IVIM values. It is known that the perfusion fraction f found in the biexponential IVIM model depends on TE.[24] A similar effect was observed for f_1 and f_2, which both were reported to decrease by ~40% in the liver if the TE is reduced from 100 ms to 50 ms.[25,26] Therefore, we assume here that f_1 and f_2 scale identically with the TE and the following values were used in the optimization: $(f_1, f_2) = \{1.0 \cdot (17.0\%, 13.7\%), 0.8 \cdot (17.0\%, 13.7\%), 0.6 \cdot (17.0\%, 13.7\%)\}$. The factors 1.0, 0.8, and 0.6 shall account for a TE range of ~45-100 ms.[24,26] The absolute values for f_1 and f_2 (i.e., 17.0% and 13.7%) were set to the mean of the values measured in the 10 first volunteers of Riexinger et al.[15] Concerning the pseudo-diffusion coefficients, we assumed that their true values might be larger or smaller than reported in Riexinger et al[15] given their large fit uncertainty. Hence, $D_1^* = 0.085\text{mm}^2/\text{s} \cdot \{0.6, 1.0, 1.4\}$ and $D_2^* = 2.55\text{mm}^2/\text{s} \cdot \{0.6, 1.0, 1.4\}$ was used and all 9 combinations of these values were probed. Taken together with the 3 combinations for the perfusion fractions, this amounted to 27 combinations of triexponential IVIM parameters. The tissue diffusion coefficient was set to 0.0012 mm^2/s.

2.3 | Evaluation of b-value distributions

The evaluation of the quality of a b-value distribution was based on the summed relative error $\sigma_{\text{sum}} = \sum_{\text{IVIM parameter set}=1}^{27} \left(\sigma_{f_1} + \sigma_{f_2} + \sigma_{D_1^*} + \sigma_{D_2^*} + \sigma_D\right)$. The individual relative errors are defined with respect to their ground truth values, for example, for f_1:

$$\sigma_{f_1} = \frac{1}{f_1}\sqrt{\frac{1}{N}\sum_{i=1}^{N}\left(f_{1,i} - f_1\right)^2}. \quad (3)$$

Here, $f_{1,i}$ is the f_1 value obtained from signals that were computed according to Equation 2. Before the fit was performed, Gaussian noise was added to the complex signal to simulate a Rician distribution of the magnitude signal. This was performed N times with a signal-to-noise ratio (SNR) of 30, roughly matching typical in vivo SNRs.[6]

2.4 | Fitting routine

For the signal fitting, a 2-step approach was used. First, a monoexponential function $S(b) = S(0) \cdot \exp(-b \cdot D)$ was fitted using only b-values above 200s/mm^2 and starting points $S(0) = 0.8$, $D = 0.001$ mm^2/s to estimate the tissue diffusivity D. Fixing this D value, in the second step, a triexponential signal curve (Equation 2) was fitted to the signal. For this purpose, the signal was normalized by the mean of all $\text{b} = 0$ s/mm^2 signals to ensure $S(0) = 1$ and to reduce the number of fit parameters. The triexponential fit was performed using the MATLAB function lsqcurvefit (starting points: $f_1 = f_2 = 10\%$, $D_1^* = 0.5$ mm^2/s, $D_2^* = 10$ mm^2/s; lower bound: $f_1 = f_2 = 1\%$, $D_1^* = 0.01\,\text{mm}^2/\text{s}$, $D_2^* = 0.01\,\text{mm}^2/\text{s}$; upper bound: $f_1 = f_2 = 50\%$, $D_1^* = 5$ mm^2/s, $D_2^* = 20$ mm^2/s). The perfusion fractions represent the signal arising from blood. Because only a maximum of 100% of the signal may arise from blood, the sum of upper boundaries was equal to 100%. Because we did not want to favor 1 of the fractions, we set their upper limits to 50%.

The upper limits of the pseudo-diffusion coefficients were set at least 8-fold higher than their expected value based on reference.[15]

2.5 | Optimization

In the optimization, the optimized b-values were chosen from a predefined set of 64 b-values (minimal value: step size: maximum value; 0:0.1:2; 2.5:0.5:5; 6:1:10; 15:5:100; 150:50:800 in units of s/mm^2).

First, an initial distribution consisting of 6 b-values was generated. Then additional optimized b-values were added consecutively. Figure 1 shows a flow chart of the process.

2.6 | Step 1: initial distribution

The initial distribution was chosen by generating 1000 random and unique b-value distributions. Distributions whose fit did not converge were considered as suboptimal and were, therefore, discarded. To ensure that the signal normalization could be performed, at least 1 b-value with $b = 0$ s/mm^2 was specified. N was initially set to 20. In a second step, all distributions whose σ_{sum} was smaller than twice the minimal σ_{sum} of all considered distributions were tested a second time with $N = 40$. The distribution with the lowest σ_{sum} was further optimized by replacing 1 b-value (except $b = 0$ s/mm^2) consecutively with the other allowed b-values (with $N = 2000$). In this step, to speed up the process, only every third b-value of the predefined 64 b-values were tested first. The 4 b-values around the b-value with minimal σ_{sum} were tested and the distribution with the lowest σ_{sum} was selected as a new optimized distribution. This step was performed for each b-value and repeated 5 times. The resulting b-value distribution was used as initial b-value distribution.

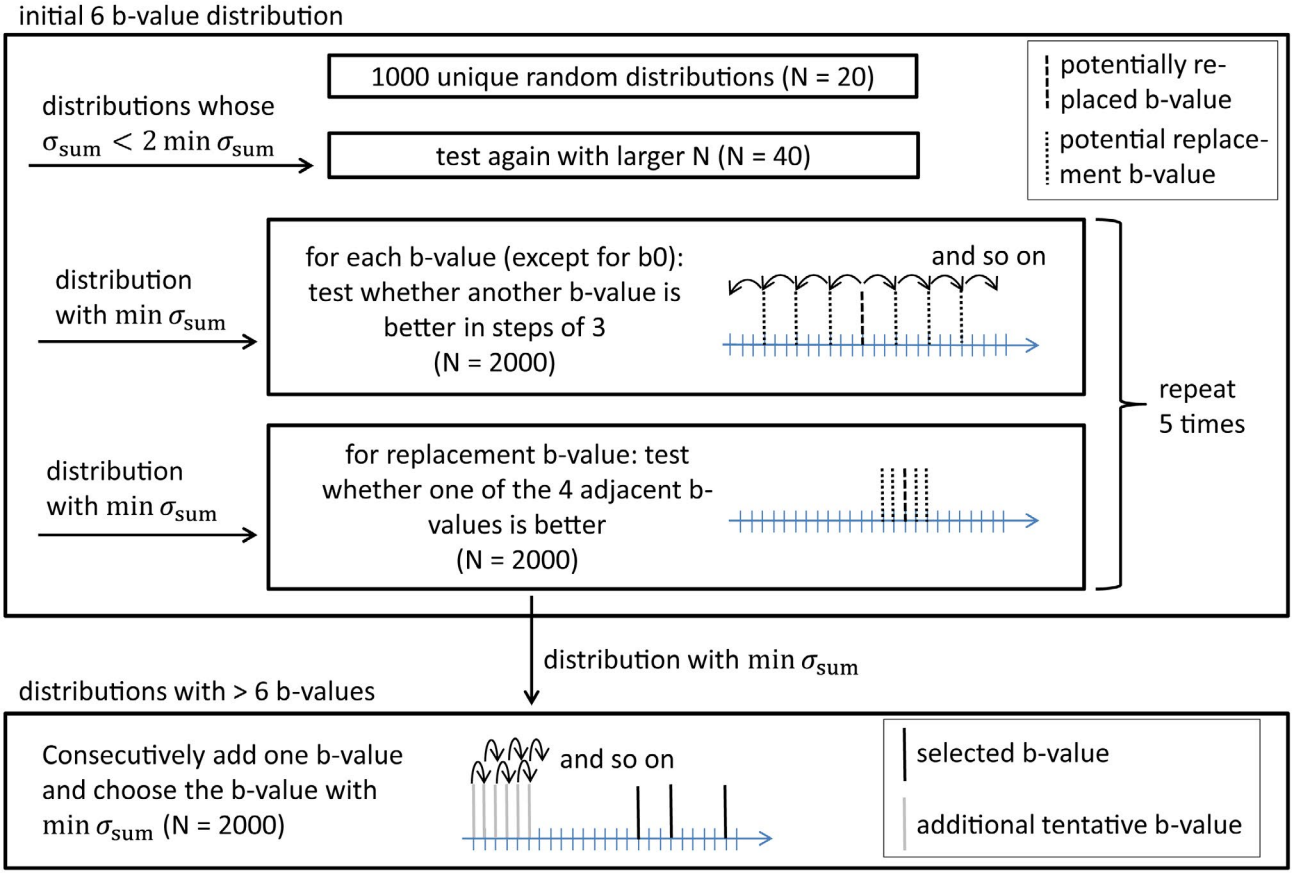

FIGURE 1 Optimization scheme: first, an initial 6 b-value distribution was generated. Additional b-values were consecutively added until a set of 100 optimized b-values was obtained

TABLE 2 b-Value distributions used for evaluation

Distribution	b-values [s/mm^2]
$\{b_{lit1}\}^{23}$	0, 10, 20, 40, 90, 100, 170, 200, 210, 240, 390, 530, 620, 750, 970, 1000
$\{b_{lit2}\}^{10}$	0, 5, 10, 15, 20, 25, 30, 35, 40, 45, 50, 100, 200, 400, 600, 800
$\{b_{lit3}\}^{6}$	0, 0, 10, 10, 10, 40, 70, 130, 170, 190, 240, 190, 240, 740, 830, 1000
$\{b_{opt}\}$ (first 16 b-values)	0, 0.3, 0.3, 70, 200, 800, 70, 1, 3.5, 5, 70, 1.2, 6, 45, 1.5, 60
17th to 40th b-value	1.8, 10, 700, 0.2, 2, 25, 6, 35, 2, 6, 7, 1.6, 25, 0.2, 1.7, 200, 1.5, 8, 0.2, 0.2, 9, 0, 800, 9
41st to 60th b-value	70, 1.6, 95, 15, 700, 1.8, 200, 0.2, 1.2, 45, 0.9, 1.2, 0.2, 0.2, 1.8, 5, 0, 8, 35, 1.6
61st to 80th b-value	7, 0.2, 1.3, 0.3, 5, 0.2, 7, 50, 0, 95, 1.9, 650, 250, 90, 150, 6, 0.4, 200, 800, 1.5
81st to 100th b-value	1.7, 0.2, 3.5, 0, 75, 0.3, 25, 1.1, 6, 550, 0.9, 4, 1.8, 700, 85, 200, 0, 1.2, 10, 1.8

Optimized b-values are listed in the order they appeared in the optimization.

2.7 | Step 2: adding of optimal b-values

Starting from the initial b-value distribution, distributions with more b-values were found by iteratively adding 1 new b-value. Each allowed b-value was tested once and the new b-value was set to the b-value with minimal σ_{sum} using $N = 2000$. This process was repeated until a distribution of 100 b-values was found.

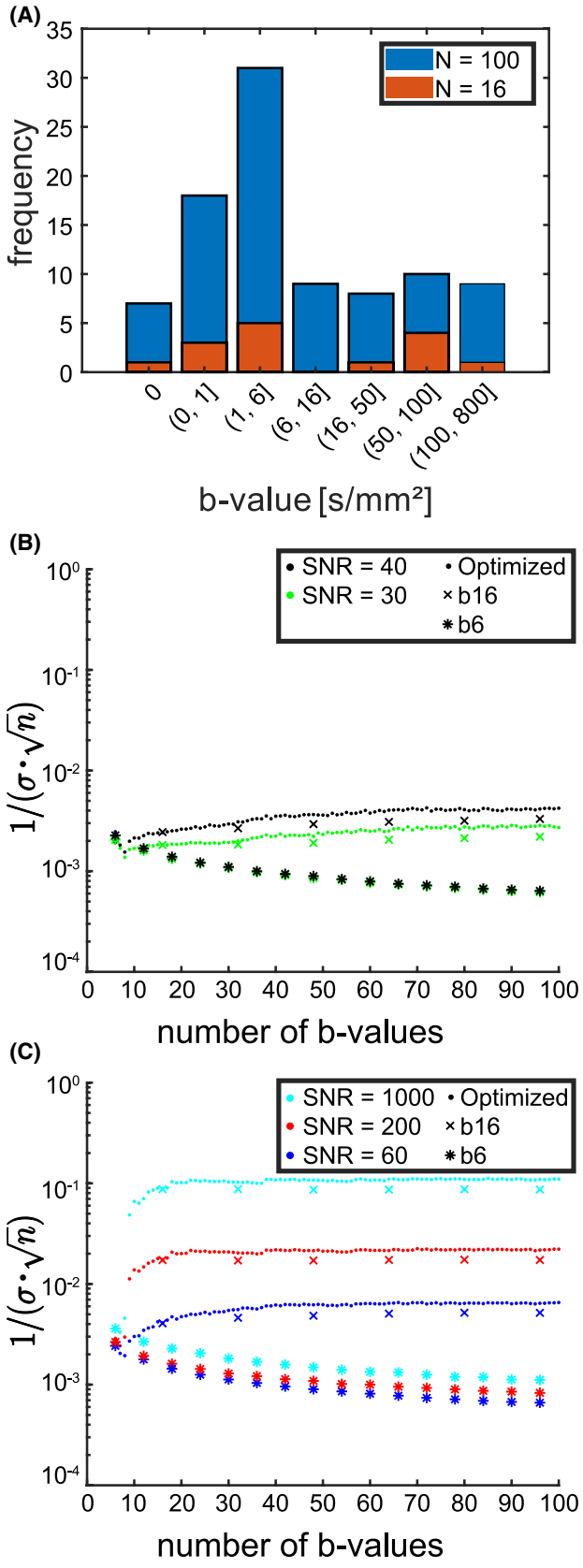

FIGURE 2 (A) Frequency of optimized b-values grouped in 7 intervals. (B and C) Simulation of the time-normalized fit quality of a subset of the optimized b-value distribution (•), and the repeated use of the initial 6 (*) and 16 (x) b-values for a SNR of (B) 30, 40, (C) 60, 200, and 1000. The subset of the optimized b-value distribution contains the respective number of b-values, which were chosen according to the order they appeared in the optimization. An increase of $1/\left(\sigma\sqrt{n}\right)$ indicates a better improvement of fit stability than obtained for linear fits, with the number of acquired b-values n

2.8 | Step 3: evaluation

To evaluate the time-normalized fit quality $\left(\sigma_{sum}\sqrt{n}\right)^{-1}$, where n is the number of b-values, was calculated with $N = 2000$ to evaluate the performance of the here optimized distribution. The dependence of the time-normalized fit quality on n was evaluated for SNR equal to 30, 40, 60, 200, and 1000. For this purpose, the first 6 to 100 b-values of the optimized distribution were used. An alternative approach to using a large number of optimized b-values would be to use only, for example, 6 or 16 b-values and to spend the acquisition time on signal averages. To evaluate the performance of this alternative approach, the first 6 b-values of the optimized distribution were simulated with a range of repetitions (i.e., amounting effectively to 12, 18, 24, etc. b-values). The same was done with the first 16 b-values.

Three b-value distributions were taken from the literature,[6,10,23] which all featured 16 b-values (Table 2) and were compared to the here optimized first 16 b-values. For each of the distributions, σ_{sum}, σ_{f_1}, σ_{f_2}, $\sigma_{D_1^*}$, and $\sigma_{D_2^*}$ were computed for SNR ranging from 5-200 in steps of 5.

For 1 IVIM parameter set ($f_1 = 17\%$, $f_2 = 13.7\%$, $D = 0.0012$ mm^2/s, $D_1^* = 0.085$ mm^2/s, $D_2^* = 2.55$ mm^2/s) and 5 different SNRs (30, 40, 50, 60, 200), 95% confidence intervals of the fitted IVIM parameters were computed. Therefore, the same fitting procedure as described in "Fitting routine" was used, except for the use of the MATLAB fit-option *multistart* to generate 99 additional starting points. Because confidence intervals cannot be computed by the use of the MATLAB function *multistart*, a single fit identical to the *multistart* fit using only the best start parameters found by the *multistart* approach, was used. For each IVIM parameter and each number of b-values, the median of the 95% confidence limits estimated by the fit were calculated over all N. Once, the optimized b-values were used (with 6 to 100 b-values). Once, $\{b_{lit2}\}$ was used, which is a b-value distribution taken from

literature featuring 16 b-values. As above, a range of repetitions was used in this case (i.e., amounting effectively to 32, 48, 64, etc. b-values). $N = 500$ was chosen. Additionally, the Akaike's information criterion (AIC) was computed with 3 SNRs (30, 60, 200) for the optimized b-value distribution (again with $N = 500$) to compare the bi- and triexponential fit.

2.9 | In vivo IVIM measurements

The liver of 3 healthy volunteers were examined on a 3T scanner (Magnetom Prisma; Siemens Healthcare Erlangen, Germany) with an 18-channel body coil and 4 different distributions of 16 b-values ($\{b_{lit1}\}$, $\{b_{lit2}\}$, $\{b_{lit3}\}$, 16 first b-values of $\{b_{opt}\}$, see Table 2) as well as with the full distribution of

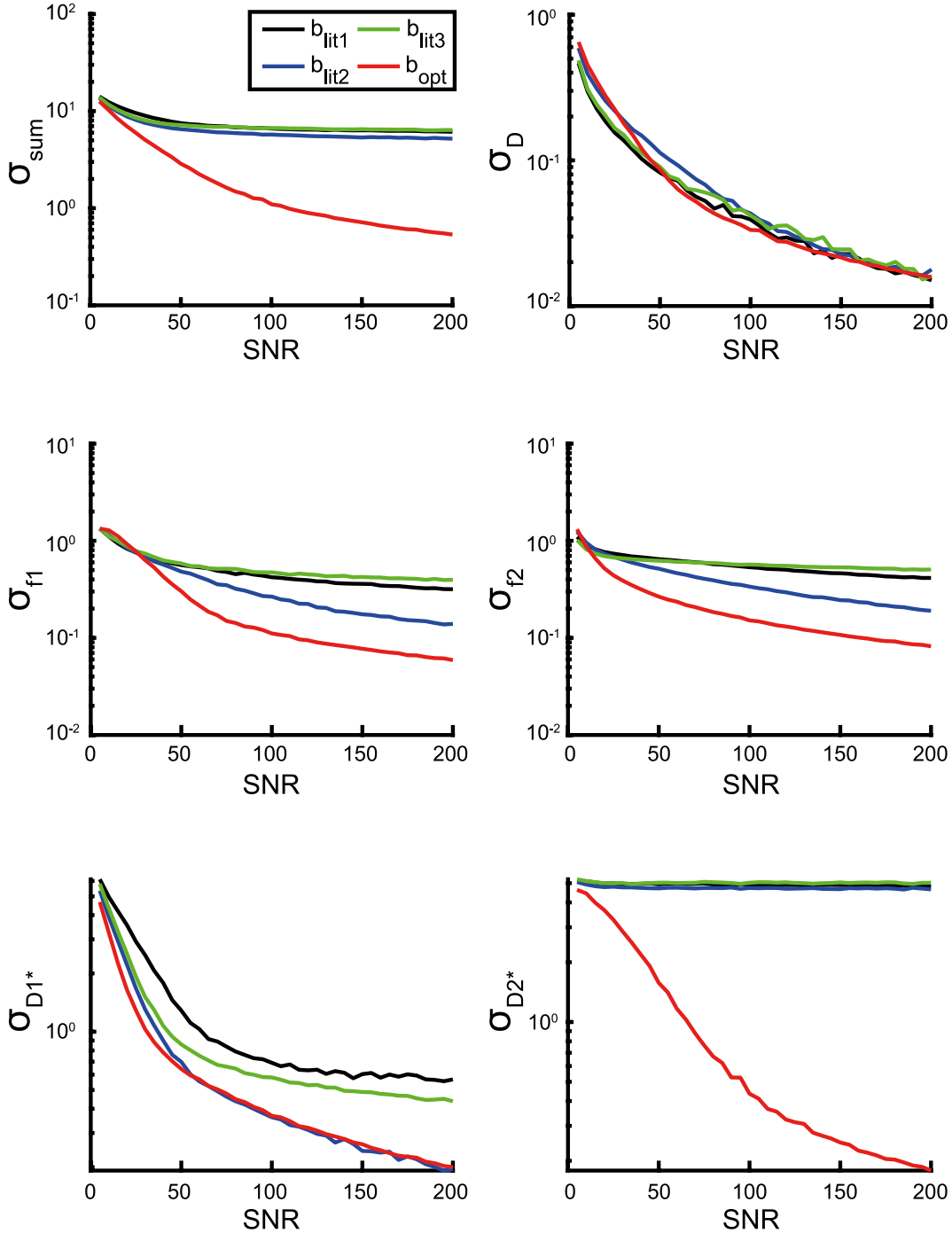

FIGURE 3 Simulated relative errors at different levels of SNR for 3 representative b-value distributions found in literature containing 16 b-values and for numerically optimized set of 16 b-values

100 optimized b-values used as reference. The study protocol was approved by the local institutional ethics committee and written informed consent was obtained from all participants.

Diffusion-weighted images were acquired with respiratory triggering, an isotropic voxel size of $4 \times 4 \times 4$ mm^3, a field of view of 400×400 mm^2, 6 transversal slices, slice gap

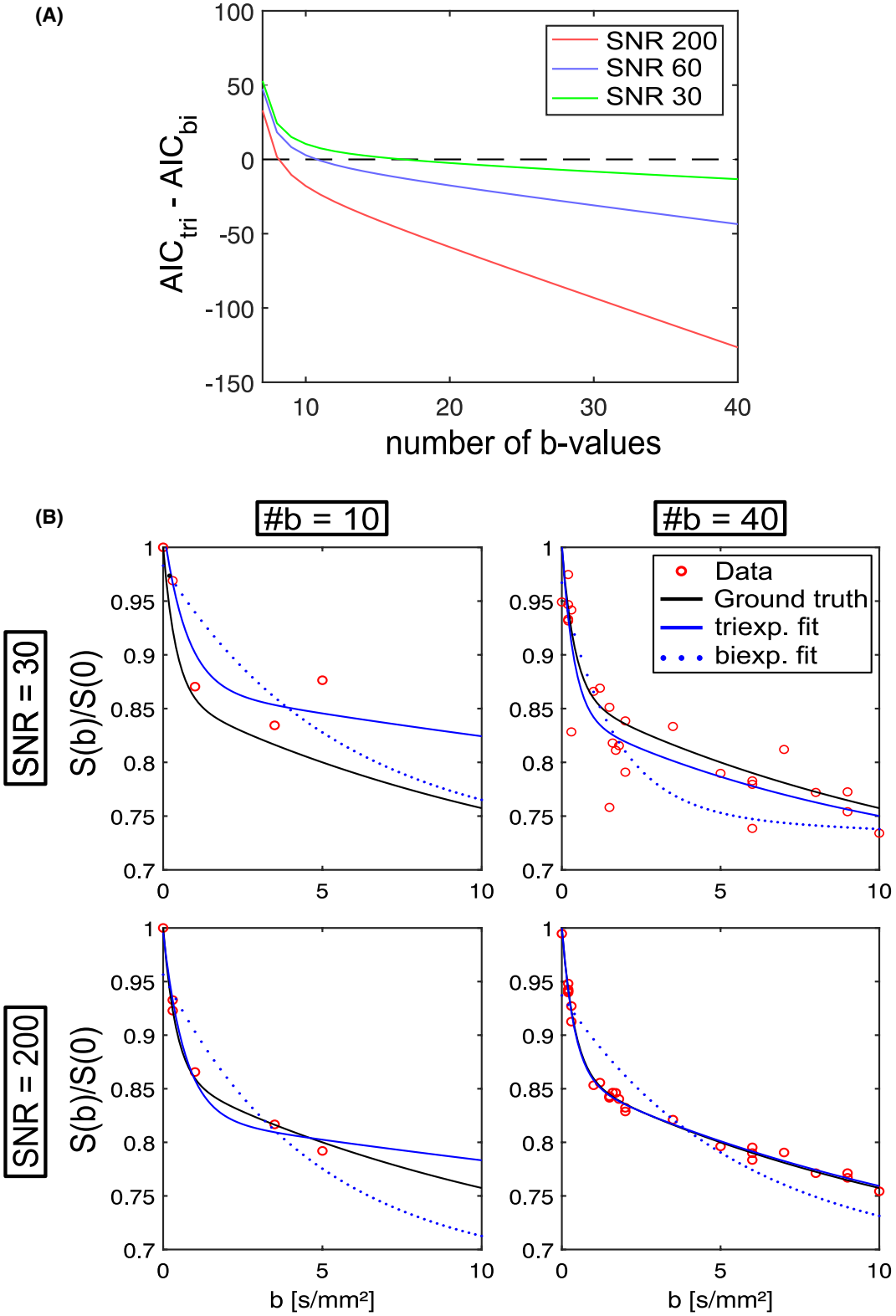

FIGURE 4 (A) Difference of AIC-values calculated for the bi- and triexponential fit with simulated data and SNRs of 30, 60, and 200. Negative values indicate that the triexponential IVIM curve is more likely the correct one for describing the data than the biexponential curve. (B) Simulated data (o) with the ground-truth signal (black line) and a bi- (dotted blue line) and triexponential (straight blue line) fit for SNRs of 30 and 200 as well as 10 and 40 b-values

of 4 mm, a partial Fourier factor of 0.75 along the phase-encoding direction, a readout bandwidth of 2272 Hz/Px, effective repetition time (trigger duration) = 2500 ms, TE = 45 ms, fat saturation by spectral attenuated inversion recovery (SPAIR), and echo planar readout accelerated by parallel imaging (GRAPPA, acceleration factor of 2, 24 autocalibration lines). Diffusion gradients were applied along tetrahedral diffusion directions (1, −1, 1), (−1, −1, 1), (−1, −1, −1), and (1, −1, −1), which are stated in the scanner coordinate system. The distribution of 100 optimized b-values had a total acquisition time of 38:52 min. The 4 chosen b-value distributions featuring 16 b-values were measured consecutively with a total acquisition time of 4:48 min for each distribution.

Effective b-values were subsequently calculated taking into account the impact of imaging gradients (the impact of imaging gradients on the IVIM parameter estimation is shown in Supporting Information Figure S1). This effect is most pronounced for the small b-values. The effective b-values were 0.15, 0.216, 0.298 s/mm^2 for the nominal values b = 0, 0.2, 0.3 s/mm^2, respectively. In each slice, a region of interest (ROI) was positioned in the first unweighted image, avoiding major blood vessels and only including

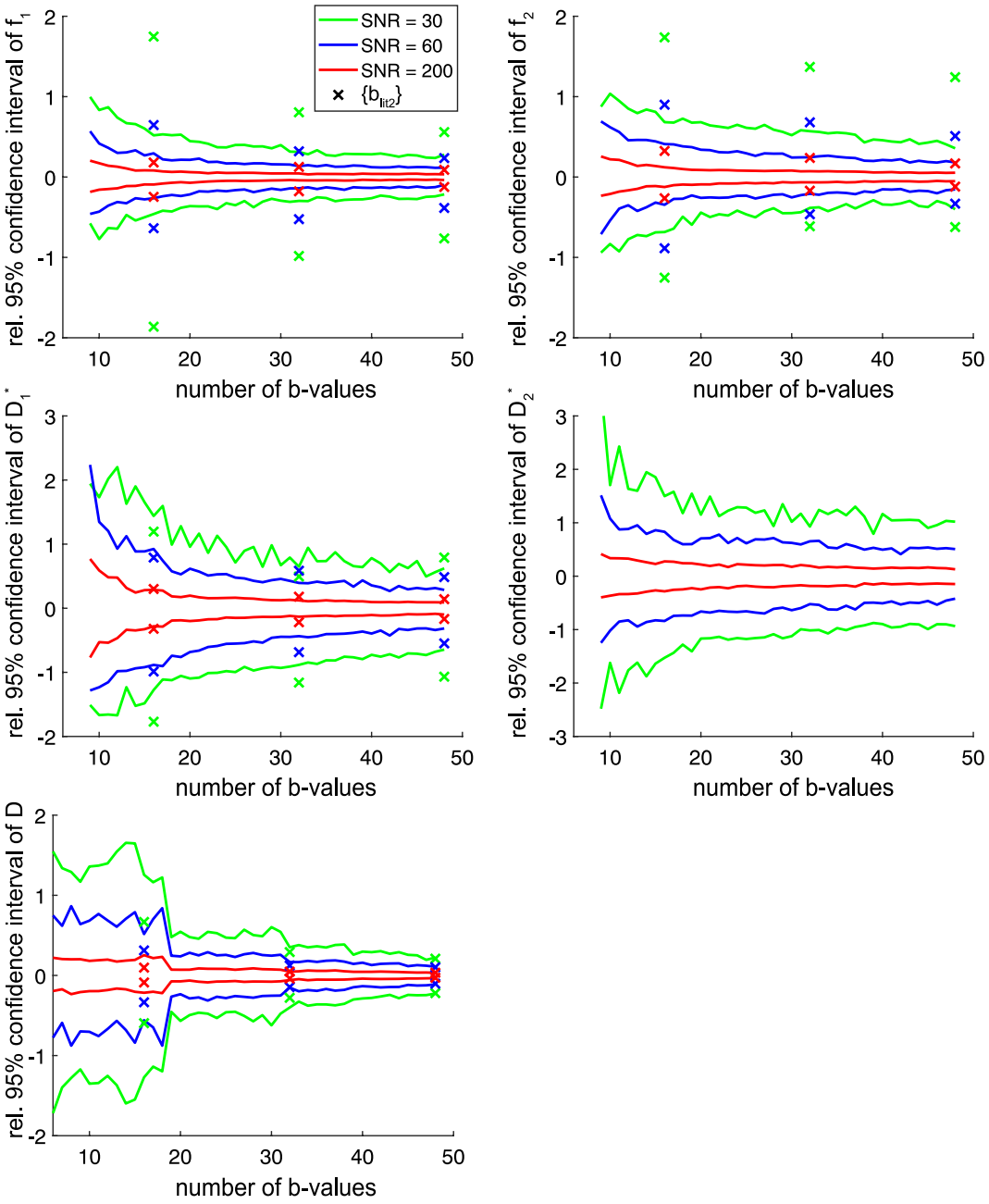

FIGURE 5 Median of upper and lower limit of relative 95% confidence intervals (normalized by the true value, that is, for example, for the upper limit of f_i: (median(upper limit of CI_{f1}) − $f_{1,true}$)/$f_{1,true}$ is plotted) of the optimized b-value set (lines) and multiples of $\{b_{lit2}\}$ (x). The confidence interval of D_2^* estimated with $\{b_{lit2}\}$ were orders of magnitudes higher and therefrom omitted to achieve a better readability

liver tissue. The signal was calculated using the median intensity over all diffusion directions inside the ROI. It was then normalized to the mean of the unweighted signals. The entire data set, acquired with all 100 optimized b-values, and the 4 individual data sets consisting of 16 b-values each, were fitted with the above described fitting routine (see section "Fitting routine"), which was identical except for the use of the MATLAB fit-option *multistart* to generate 999 additional starting points and an additional biexponential fit to calculate AIC values and compare the bi- and triexponential fit. Because a reliable ground truth was not available for in vivo measurements, the fitted parameters of the distribution of 100 optimized b-values were used as reference. For each IVIM parameter obtained with the distributions consisting of 16 b-values, the root mean square deviation to the reference values were calculated. Afterward, they were summed to compute a total relative error. Additionally, a pixel-wise evaluation for all slices for 1 volunteer was performed using the same fitting routine.

The SNR of each volunteers' liver parenchyma at b = 0 s/mm^2 was estimated by the differential method[27,28] applicable for images acquired with parallel imaging. Two circular ROIs were drawn on each slice into the right liver lobe on the 2 unweighted acquisitions closest in time. The SNR for each ROI was calculated as follows:

$$\mathrm{SNR} = \frac{\mathrm{mean}\left(S_1 + S_2\right)}{\sqrt{2}\ \mathrm{std}\left(S_1 - S_2\right)}, \tag{4}$$

where S_1 and S_2 are the signal values in each ROI for both time points. The estimated mean SNR of all ROIs in 1 volunteer was defined as the volunteers' SNR.

3 | RESULTS

The optimized distribution of b-values is listed in Table 2 and illustrated in Figure 2A. The initial 6 b-values feature 3 small b-values (≤ 0.3 s/mm^2), the medium b-values 70 and 200 s/mm^2, and 1 large b-value (800 s/mm^2). For larger *N*, this pattern disappears and b-values in the range from 1 s/mm^2 to 50 s/mm^2 are chosen more frequently compared to b-values above 50 s/mm^2. The density at very small b-values <1 s/mm^2 is much larger than at higher b-values.

The time-normalized fit quality of the optimized b-value distribution as a function of the number of b-values *n* is shown in Figures 2B,C (using the optimized b-values according to the order they appeared in the optimization). Independently of the SNR, the time-normalized fit quality can be increased by the use of more b-values when the number of b-values is small, for example, less than ~20 b-values for SNR = 200. This indicates that one gains more than the usual square root of time increase in fit stability found for linear fits; and that one should use more than 6 b-values. A distribution of 100 optimized b-values performed better than repeated acquisitions with distributions of either 6 or 16 optimized b-values. Using the 6 b-value distribution is not recommendable because averaging the data multiple times does decrease the time-normalized fit quality.

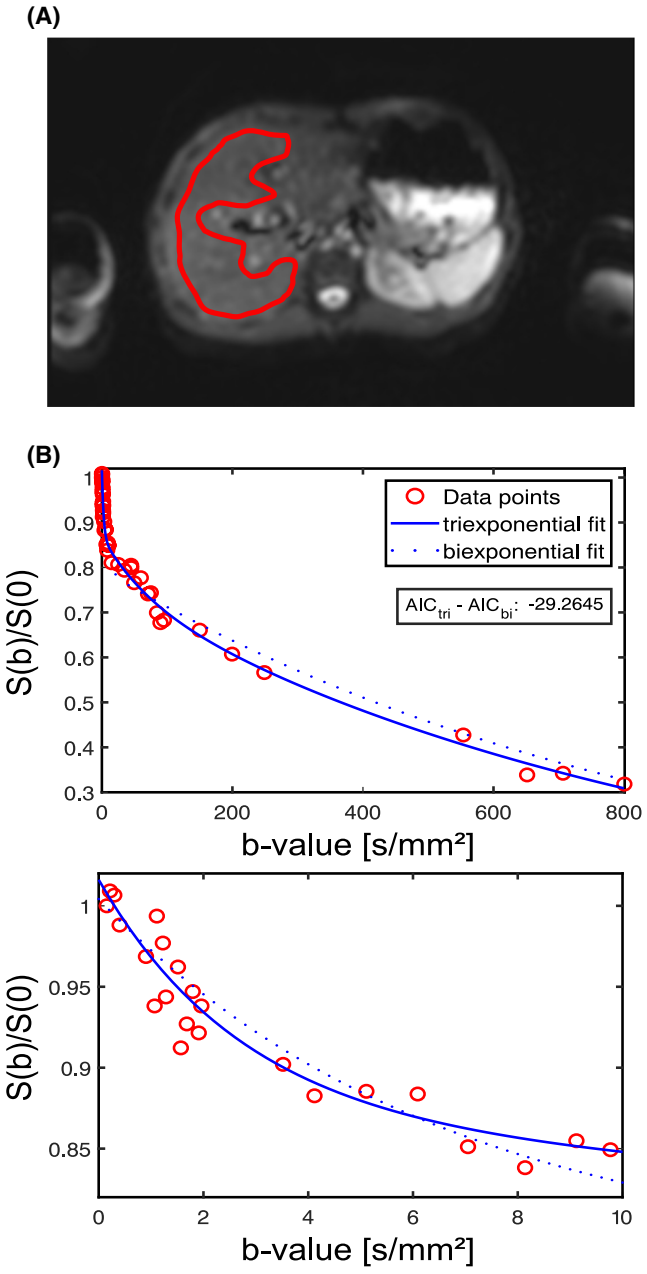

FIGURE 6 (A) Sample image data of 1 volunteer and the used ROI plotted in red (b = 0.2 s/mm^2). Normalized signal attenuation of 1 representative volunteer and slice. Left: full b-values range. Right: zoomed view of the same data. Markers represent measured data, lines represent the fitted bi- and triexponential model. The difference of calculated AIC-values is negative, indicating the triexponential model is more favorable

Figure 3 shows the comparison of $\{b_{opt}\}$ to the b-value distributions taken from the literature. The diffusion coefficient is well-determined by each of the 4 considered 16-b-value distributions, whereas large differences were found when fitting IVIM parameters. $\{b_{lit2}\}$ performed better than $\{b_{lit1}\}$ and $\{b_{lit3}\}$ for estimating f_1 and f_2, but not as good as $\{b_{opt}\}$. This behavior can be explained by the b-values included in the distribution. The smallest b-value used by $\{b_{lit1}\}$ and $\{b_{lit3}\}$ is 10 s/mm^2, which seems to be too high for determining the perfusion fractions correctly. For D_1^*, $\{b_{lit2}\}$ and $\{b_{opt}\}$ performed equally well and much better than the other 2 distributions. A b-value of 5 s/mm^2, therefore, appears to be sufficiently small to ensure decent fit precision for D_1^*. For D_2^*, only $\{b_{opt}\}$ performed well. Because the initial signal drop, which is linked to the pseudo-diffusion coefficient of the fast compartment, occurs for $b < 1$ s/mm^2, $\{b_{lit1}\}$, $\{b_{lit2}\}$, and $\{b_{lit3}\}$ were not suited to fit D_2^*.

Figure 4 shows the difference of AIC values obtained with bi- and triexponential fit in dependence of the number of b-values taken from the optimized distribution. Negative values in Figure 4 indicate that the triexponential fit represents the data better. If the number of b-values is small, the biexponential fit represents the data better. If more b-values are used, the opposite holds true. With increasing SNR, less b-values are needed to favor the triexponential fit.

In Figure 5, the medians of the upper and lower limit of the relative confidence intervals of the triexponential fit are shown. Similar to the time-normalized fit quality, the confidence interval decreases with increased SNR and number of b-values. Even for low SNRs, the perfusion fractions f_1 and f_2, as well as the pseudo-diffusion coefficient D_1^* can be roughly estimated. However, for estimating the fast pseudo-diffusion coefficient D_2^*, more b-values are needed for lower SNR. The confidence interval of the diffusion

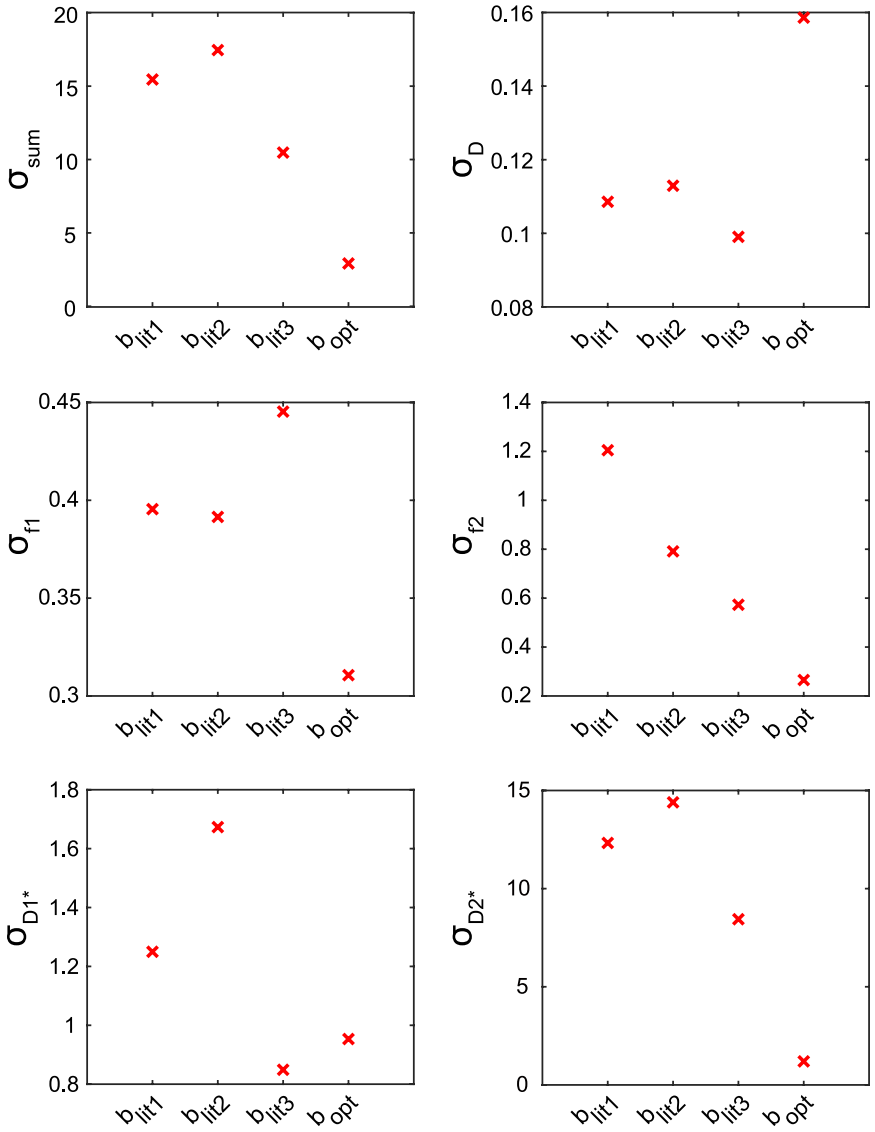

FIGURE 7 Relative errors for 3 representative b-value distributions found in literature containing 16 b-values and for numerically optimized set of 16 b-values (in vivo measurements). The relative errors were computed with respect to an optimized b-value distribution containing 100 b-values

coefficient is more or less constant and is strongly reduced at 19 b-values. This can be explained by the addition of a high b-value to the distribution.

3.1 | In vivo measurement

The estimated SNR was 65, 68, and 72 for the 3 volunteers. Sample image data of 1 volunteer and the used ROI are shown in Figure 6A. The respective signal attenuation curves are plotted in Figure 6B, with the performed bi- and triexponential fit and their corresponding AIC-values. $AIC_{tri} - AIC_{bi}$ is negative, indicating that the triexponential IVIM function is better suited to describe the data than the biexponential function.

The group averaged estimated triexponential IVIM parameters of the optimized data set were:

$$D = 0.0011 \pm 0.00024 \text{mm}^2/\text{s}, f_1 = 13.1 \pm 4.5\%, f_2 = 10.8 \pm 1.6\%, D_1^* = 0.016 \pm 0.007 \text{mm}^2/\text{s}, D_2^* = 0.50 \pm 0.224 \text{mm}^2/\text{s}. \quad (5)$$

Standard deviations and mean values were calculated among all volunteers and slices. The relative errors and the summed relative error for each investigated b-value distribution, computed with respect to the distribution of 100 optimized b-values, is illustrated in Figure 7. The diffusion coefficient is well determined by all distributions, but the optimized distribution is slightly more inaccurate presumably because of the lower number of high b-values. The perfusion fractions f_1 and f_2 and the fast pseudo-diffusion coefficient D_2^* were determined best by the optimized distribution. The perfusion fractions and D_1^* had the lowest relative errors with $\{b_{opt}\}$, whereas the slow pseudo-diffusion coefficient D_1^* is determined best with $\{b_{lit2}\}$, which had been optimized for biexponential IVIM. By far, D_2^*

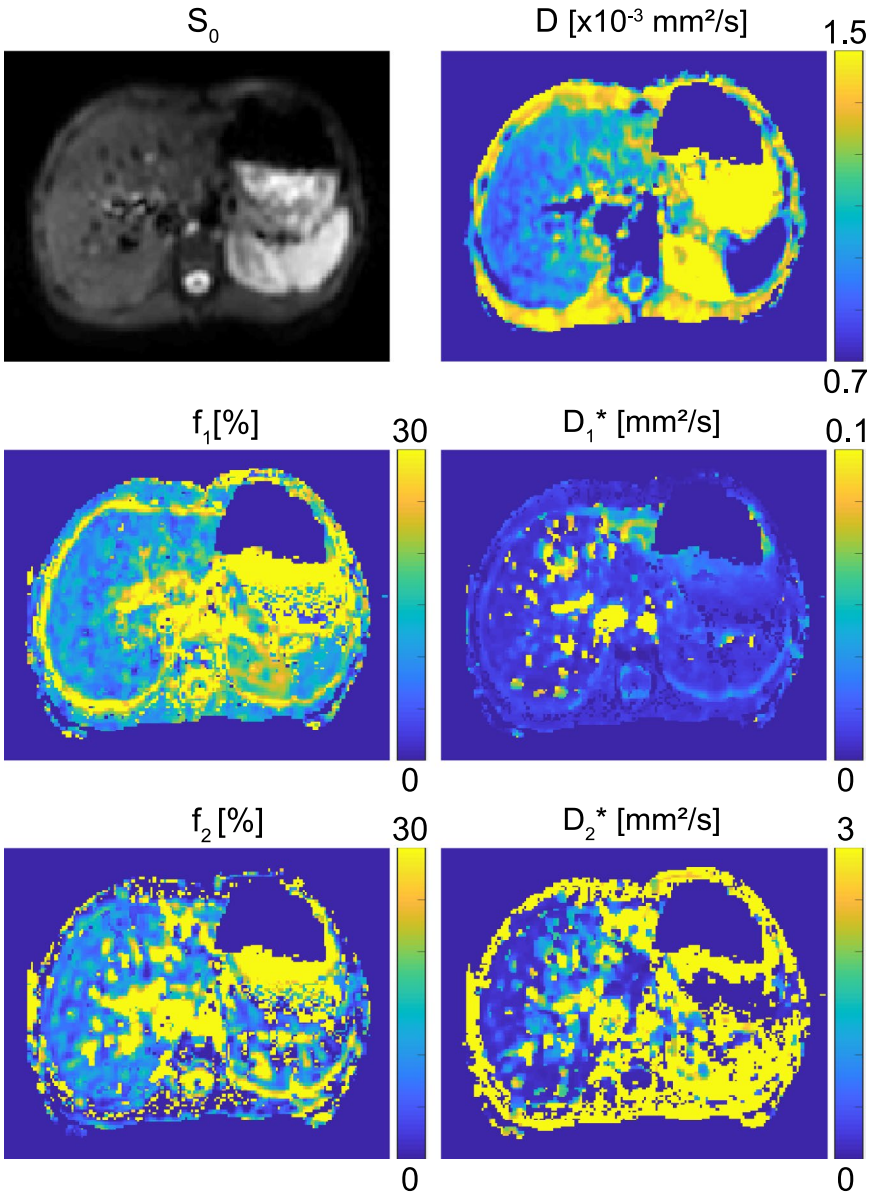

FIGURE 8 IVIM-maps from 1 representative slice and volunteer calculated with the full set of 100 optimized b-values

can be determined best with $\{b_{opt}\}$ and it dominates, moreover, the summed relative error. The low b-values contained in $\{b_{opt}\}$ appear to be crucial for reliably determining D_2^*.

IVIM parameter maps could sucessfully be calculated for all slices using the set of 100 optimized b-values. Maps of 1 representative slice are shown in Figure 8 with the corresponding unweighted image. Within the liver, D increases in the left liver lobe, because of the pulsation artifact.[29,30] f_1 seems homogeneously distributed across the whole liver. Bright spots are located in the vicinity of large vessels. f_2, D_1^*, and D_2^* also exhibit bright spots close to vessels, which are more prevalent than in the f_1 map. Within those spots, the pseudo-diffusion coefficients increase drastically compared to the surrounding tissue. For the slow pseudo-diffusion coefficient, this increase is from 0.006 mm^2/s (liver parenchym) up to 1 mm^2/s (big vessel). The fast diffusion coefficient increases from a minimum of 0.1 up to 19 mm^2/s. Maps computed with 16 b-values are shown in Supporting Information Figure S2 for the first 16 optimized b-values and in Supporting Information Figure S3 for $\{b_{lit2}\}$. In particular the quality of the D_2^* map decreases if only 16 b-values are used.

4 | DISCUSSION AND CONCLUSIONS

The purpose of this study was to find an optimized b-value distribution for triexponential IVIM in the liver. For the biexponential IVIM model, b-value optimizations were already performed for different organs and purposes to increase IVIM parameter reproducibility.[6,31-34] Besides the optimization of the b-value sampling, lots of other optimizations for the biexponential IVIM model in the liver, for example, concerning breathing schemes or minimizing the acquisition time were performed.[34-39] However, to our knowledge, no comparable optimization has been performed for triexponential IVIM yet. Within this study, we were able to find an optimized distribution of b-values for triexponential IVIM in the liver and demonstrated the advantage of optimized b-values compared to 3 representative b-value distributions used in literature by means of simulations and volunteer measurements. In contrast to b-value distributions used in literature,[6,10,13] our results would suggest that for accurate triexponential IVIM measurements, frequent acquisition of very small b-values (<6 s/mm^2) is required. This recommendation is supported by the work of Cohen et al.[21] They showed that the pseudo-diffusion coefficient in the biexponential IVIM model is underestimated, if too few small b-values are acquired, which confirms our finding for the triexponential model. Additionally, pseudo-diffusion coefficients exhibit low reproducibility.[40] Therefore, by spending more time on measuring very small b-values, where the signal is highly sensitive to the pseudo-diffusion effects, one can increase the fit precision of triexponential IVIM parameters.

Although the summed relative error within the simulation is dominated by the relative error of the fast pseudo-diffusion coefficient, the other triexponential IVIM parameters were also estimated best by the optimized b-value distribution, except for the slow pseudo-diffusion coefficient, which is estimated best by the b-value distribution optimized for biexponential IVIM by Lemke et al.[6] In our work, only 16 b-values were used for the in vivo measurement for comparison and evaluation of the full optimized b-value distribution. Using more b-values, one can further increase the fit precision by decreasing the confidence interval as shown above. However, the time-normalized fit quality predicts the largest improvement in the range of 10 to 20 b-values for all considered SNRs. Therefore, we would recommend acquiring at least 16 b-values for triexponential IVIM exams of the liver.

The estimated mean pseudo-diffusion coeffiecients D_1^* and D_2^* in the volunteers study were smaller than the ones used as ground-truth values within the optimization. This might be explained by the different slice orientation (axial here, sagittal in Riexinger et al).[15] Another explanation might be the presence of different inflow effects because of the use of respiratory triggering compared to free breathing in Riexinger et al.[15] Free breathing might also lead to inclusion of contributions from larger vessels in the ROI, which presumably leads to increased pseudo-diffusion coefficients. This effect is highlighted in the estimated IVIM maps (Figure 8), where an inhomogenious behaviour of IVIM parameter across the liver and bright spots are clearly observable. These spots are most presumably to be attributed to large vessels. If a ROI-wise evaluation is performed, the amount of larger vessel will have a critical impact on measured pseudo-diffusion coefficients. Optimized b-values for the IVIM parameters determined in this study are provided as supplemental material (Supporting Information Table S1). The origin of the observed discrepancy between estimated and ground-truth values is most likely a mixture of issues mentioned above. This illustrates the difficulty of producing triexponential IVIM parameter across different studies and should be the subject of further investigations.

We acknowledge several limitations of this study. First, we did not evaluate the optimized distribution within a clinical study. Although the optimization considered varying IVIM parameters, the optimal b-value distribution for assessment of diseased tissues might differ. Second, the optimized b-value distribution added 1 b-value consecutively instead of optimizing b-value distributions with a fixed number of b-values. Potentially a full optimization carried out for each particular number of b-values might have yielded further improved distributions. Third, in vivo examinations were performed with a comparatively short TE (TE = 45 ms), and

therefore the evaluation presented in Figure 2B may differ for longer TEs, commonly required on clinical MRI systems. Fourth, the superior performance of the optimized b-value distribution compared to other distributions was only shown for 3 healthy volunteers. Although this study focused on imaging of the liver, the kidney also shows a triexponential signal behaviour.[11-13] One could, therefore, optimize a b-value distribution for both, the kidney and the liver in parallel. In the optimization, the nominal value $b_0 = 0$ s/mm^2 was used. An optimization using the sequence-dependent actual b_0 value—including the effect of imaging gradients—might yield a further improved b-value distribution. Fifth, this optimization was focused on ROI-wise evaluations. For voxel-wise evaluations, it would presumably better to vary the pseudo-diffusion coefficient within the optimization by more than ±40%. Sixth, the relative errors in Figure 7 do not allow a clear separation between an increase in precision or a reduced overall bias.

In conclusion, the measured triexponential IVIM parameters in liver imaging can be estimated more precisely using optimized b-values. Our results suggest acquiring data with a b-value distribution consisting of at least 16 b-values, including 30-50 % of b-values below 6 s/mm^2.

ACKNOWLEDGMENTS

Funding by the Deutsche Forschungsgemeinschaft (DFG) is gratefully acknowledged (LA 2804/12-1 and LA 2804/13-1). Open access funding enabled and organized by Projekt DEAL.

ORCID

Andreas Riexinger https://orcid.org/0000-0002-6346-3526
Frederik Bernd Laun https://orcid.org/0000-0002-9269-5609

REFERENCES

1. Le Bihan D, Breton E, Lallemand D, Aubin ML, Vignaud J, Laval-Jeantet M. Separation of diffusion and perfusion in intravoxel incoherent motion MR imaging. *Radiology*. 1988;168:497-505.
2. Andreou A, Koh DM, Collins DJ, et al. Measurement reproducibility of perfusion fraction and pseudodiffusion coefficient derived by intravoxel incoherent motion diffusion-weighted MR imaging in normal liver and metastases. *Eur Radiol*. 2013;23:428-434.
3. Jerome NP, d'Arcy JA, Feiweier T, et al. Extended T2-IVIM model for correction of TE dependence of pseudo-diffusion volume fraction in clinical diffusion-weighted magnetic resonance imaging. *Phys Med Biol*. 2016;61:N667-N680.
4. Fournet G, Li JR, Cerjanic AM, Sutton BP, Ciobanu L, Le Bihan D. A two-pool model to describe the IVIM cerebral perfusion. *J Cereb Blood Flow Metab*. 2017;37:2987-3000.
5. Kuai ZX, Liu WY, Zhu YM. Effect of multiple perfusion components on pseudo-diffusion coefficient in intravoxel incoherent motion imaging. *Phys Med Biol*. 2017;62:8197-8209.
6. Lemke A, Stieltjes B, Schad LR, Laun FB. Toward an optimal distribution of b values for intravoxel incoherent motion imaging. *Magn Reson Imaging*. 2011;29:766-776.
7. Eatesam M, Noworolski SM, Tien PC, et al. Liver diffusivity in healthy volunteers and patients with chronic liver disease: Comparison of breathhold and free-breathing techniques. *J Magn Reson Imaging*. 2012;35:103-109.
8. Celik A. Effect of imaging parameters on the accuracy of apparent diffusion coefficient and optimization strategies. *Diagn Interv Radiol*. 2016;22:101-107.
9. Gurney-Champion OJ, Froeling M, Klaassen R, et al. Minimizing the acquisition time for intravoxel incoherent motion magnetic resonance imaging acquisitions in the liver and pancreas. *Invest Radiol*. 2016;51:211-220.
10. Cercueil J-P, Petit J-M, Nougaret S, et al. Intravoxel incoherent motion diffusion-weighted imaging in the liver: Comparison of mono-, bi- and tri-exponential modelling at 3.0-T. *Eur Radiol*. 2015;25:1541-1550.
11. van der Bel R, Gurney-Champion OJ, Froeling M, Stroes ESG, Nederveen AJ, Krediet CTP. A tri-exponential model for intravoxel incoherent motion analysis of the human kidney: In silico and during pharmacological renal perfusion modulation. *Eur J Radiol*. 2017;91:168-174.
12. van Baalen S, Leemans A, Dik P, Lilien MR, Ten Haken B, Froeling M. Intravoxel incoherent motion modeling in the kidneys: Comparison of mono-, bi-, and triexponential fit. *J Magn Reson Imaging*. 2017;46:228-239.
13. Wurnig MC, Germann M, Boss A. Is there evidence for more than two diffusion components in abdominal organs?—A magnetic resonance imaging study in healthy volunteers. *NMR Biomed*. 2017;31:e3852.
14. van Baalen S, Froeling M, Asselman M, et al. Mono, bi- and tri-exponential diffusion MRI modelling for renal solid masses and comparison with histopathological findings. *Cancer Imaging*. 2018;18:44.
15. Riexinger AJ, Martin J, Rauh S, et al. On the field strength dependence of bi- and triexponential intravoxel incoherent motion (IVIM) parameters in the liver. *J Magn Reson Imaging*. 2019;50:1883-1892.
16. Cho GY, Moy L, Kim SG, et al. Evaluation of breast cancer using intravoxel incoherent motion (IVIM) histogram analysis: Comparison with malignant status, histological subtype, and molecular prognostic factors. *Eur Radiol*. 2016;26:2547-2558.
17. Murtz P, Pieper CC, Reick M, et al. Is liver lesion characterisation by simplified IVIM DWI also feasible at 3.0 T? *Eur Radiol*. 2019;29:5889-5900.
18. Novikov DS, Kiselev VG, Jespersen SN. On modeling. *Magn Reson Med*. 2018;79:3172-3193.
19. Le Bihan D, Breton E, Lallemand D, Grenier P, Cabanis E, Laval-Jeantet M. MR imaging of intravoxel incoherent motions: Application to diffusion and perfusion in neurologic disorders. *Radiology*. 1986;161:401-407.
20. Wetscherek A, Stieltjes B, Laun FB. Flow-compensated intravoxel incoherent motion diffusion imaging. *Magn Reson Med*. 2015;74:410-419.
21. Cohen AD, Schieke MC, Hohenwalter MD, Schmainda KM. The effect of low b-values on the intravoxel incoherent motion derived pseudodiffusion parameter in liver. *Magn Reson Med*. 2015;73:306-311.

22. Li YT, Cercueil JP, Yuan J, Chen W, Loffroy R, Wang YX. Liver intravoxel incoherent motion (IVIM) magnetic resonance imaging: A comprehensive review of published data on normal values and applications for fibrosis and tumor evaluation. *Quant Imaging Med Surg*. 2017;7:59-78.
23. Wurnig MC, Donati OF, Ulbrich E, et al. Systematic analysis of the intravoxel incoherent motion threshold separating perfusion and diffusion effects: Proposal of a standardized algorithm. *Magn Reson Med*. 2015;74:1414-1422.
24. Lemke A, Laun FB, Simon D, Stieltjes B, Schad LR. An in vivo verification of the intravoxel incoherent motion effect in diffusion-weighted imaging of the abdomen. *Magn Reson Med*. 2010;64:1580-1585.
25. Riexinger AW, Martin J, Kuder TA, et al. On the magnetic field and echo time dependence of the pseudo-diffusion coefficient. In proceedings of ISMRM. 2018; Paris; Abstract 0258.
26. Führes, T. *Echo Time Dependence of the Triexponential Intravoxel Incoherent Motion (IVIM) Parameters in Abdominal Organs*. Erlangen, Germany: Radiologisches Institut, Friedrich-Alexander-Universität Erlangen-Nürnberg; 2020.
27. Dietrich O, Raya JG, Reeder SB, Reiser MF, Schoenberg SO. Measurement of signal-to-noise ratios in MR images: Influence of multichannel coils, parallel imaging, and reconstruction filters. *J Magn Reson Imaging*. 2007;26:375-385.
28. Reeder SB, Wintersperger BJ, Dietrich O, et al. Practical approaches to the evaluation of signal-to-noise ratio performance with parallel imaging: Application with cardiac imaging and a 32-channel cardiac coil. *Magn Reson Med*. 2005;54:748-754.
29. Kwee TC, Takahara T, Niwa T, et al. Influence of cardiac motion on diffusion-weighted magnetic resonance imaging of the liver. *MAGMA*. 2009;22:319-325.
30. Rauh SS, Riexinger AJ, Ohlmeyer S, et al. A mixed waveform protocol for reduction of the cardiac motion artifact in black-blood diffusion-weighted imaging of the liver. *Magn Reson Imaging*. 2020;67:59-68.
31. Zhang JL, Sigmund EE, Rusinek H, et al. Optimization of b-value sampling for diffusion-weighted imaging of the kidney. *Magn Reson Med*. 2012;67:89-97.
32. Karki K, Hugo GD, Ford JC, et al. Estimation of optimal b-value sets for obtaining apparent diffusion coefficient free from perfusion in non-small cell lung cancer. *Phys Med Biol*. 2015;60:7877-7891.
33. Mürtz P, Sprinkart AM, Reick M, et al. Accurate IVIM model-based liver lesion characterisation can be achieved with only three b-value DWI. *Eur Radiol*. 2018;28:4418-4428.
34. Jalnefjord O, Montelius M, Starck G, Ljungberg M. Optimization of b-value schemes for estimation of the diffusion coefficient and the perfusion fraction with segmented intravoxel incoherent motion model fitting. *Magn Reson Med*. 2019;82:1541-1552.
35. Choi JS, Kim M-J, Chung YE, et al. Comparison of breathhold, navigator-triggered, and free-breathing diffusion-weighted MRI for focal hepatic lesions. *J Magn Reson Imaging*. 2013;38:109-118.
36. Furuta A, Isoda H, Yamashita R, et al. Comparison of monopolar and bipolar diffusion weighted imaging sequences for detection of small hepatic metastases. *Eur J Radiol*. 2014;83:1626-1630.
37. Kandpal H, Sharma R, Madhusudhan KS, Kapoor KS. Respiratory-triggered versus breath-hold diffusion-weighted MRI of liver lesions: comparison of image quality and apparent diffusion coefficient values. *AJR Am J Roentgenol*. 2009;192:915-922.
38. Boss A, Barth B, Filli L, et al. Simultaneous multi-slice echo planar diffusion weighted imaging of the liver and the pancreas: Optimization of signal-to-noise ratio and acquisition time and application to intravoxel incoherent motion analysis. *Eur J Radiol*. 2016;85:1948-1955.
39. Cieszanowski A, Pasicz K, Podgorska J, et al. Reproducibility of intravoxel incoherent motion of liver on a 3.0T scanner: Free-breathing and respiratory-triggered sequences acquired with different numbers of excitations. *Pol J Radiol*. 2018;83:e437-e445.
40. Andreou A, Koh DM, Collins DJ, et al. Measurement reproducibility of perfusion fraction and pseudodiffusion coefficient derived by intravoxel incoherent motion diffusion-weighted MR imaging in normal liver and metastases. *Eur Radiol*. 2013;23:428-434.

SUPPORTING INFORMATION

Additional Supporting Information may be found online in the Supporting Information section.

FIGURE S1 Estimated IVIM parameter in dependence of the calculated b_0 value treated naively as $b_0 = 0$ s/mm^2 with two SNRs of 60 and 200. Markers represent data points, lines represent their standard deviation

FIGURE S2 IVIM-maps of the same slice as in figure 8, acquired with the first 16 b-values of the optimized set. Parameter range of D: $0.7 - 1.5 \times 10^{-3}$ mm^2/s; f_1 and f_2: $0 - 30\%$; D_1^*: $0 - 0.1$ mm^2/s; D_2^*: $0 - 3$ mm^2/s

FIGURE S3 IVIM-maps of the same slice as in figure 8, acquired with the b-value set of b_{lit2}. Parameter range of D: $0.7 - 1.5 \times 10^{-3}$ mm^2/s; f_1 and f_2: $0 - 30\%$; D_1^*: $0 - 0.1$ mm^2/s; D_2^*: $0 - 3$ mm^2/s

TABLE S1 Optimized b-values from the group averaged IVIM parameters found within this study; optimized b-values listed in the order they appeared in the optimization

How to cite this article: Riexinger A, Martin J, Wetscherek A, et al. An optimized b-value distribution for triexponential intravoxel incoherent motion (IVIM) in the liver. *Magn Reson Med*. 2021;85:2095–2108. https://doi.org/10.1002/mrm.28582